RMP-Flutter-Induced Pedestal Plasma Transport

J.D. Callen, C.C. Hegna, University of Wisconsin, Madison, WI 53706-1609
A.J. Cole, Columbia University, New York, NY 10027

Paper TH/P4-20, IAEA Fusion Energy Conference, San Diego, CA, 8–13 October 2012

Issue To Be Addressed:

RMP-flutter-induced plasma transport[1] in H-mode pedestal tops.[2]

Theses:

- **Flow-screening averts stochastic[3] but not flutter[1] transport.**
- **RMP-flutter-induced *e* transport model has been developed.[2,4]**
- **RMP-flutter transport[1] might cause observed pedestal transport.[2]**
- **Model implications are different at low[5] and high[6] collisionality.**

[1] J.D. Callen, "Drift-Wave Turbulence Effects on Magnetic Structure and Plasma Transport in Tokamaks," Phys. Rev. Lett. **39**, 1540 (1977).
[2] J.D. Callen, A.J. Cole, C.C. Hegna, S. Mordijck, R.A. Moyer, "RMP effects on pedestal structure and ELMs," Nucl. Fusion **52**, 114005 (2012).
[3] A.B. Rechester and M.N. Rosenbluth, "Electron heat transport in a tokamak with destroyed magnetic surfaces," Phys. Rev. Lett. **40**, 38 (1978).
[4] J.D. Callen, A.J. Cole and C.C. Hegna, "Resonant-magnetic-perturbation-induced plasma transport in H-mode pedestals," UW-CPTC 11-15_rev.
[5] T.E. Evans et al., "RMP ELM suppression in DIII-D plasmas with ITER similar shapes and collisionalities," Nucl. Fusion **48**, 024002 (2008).
[6] W. Suttrop et al., "Studies of edge localized mode mitigation with new active in-vessel saddle coils in ASDEX Upgrade," PPCF **53**, 124014 (2011).

RMPs Reduce DIII-D Pressure Gradient At Pedestal Top

- RMP-induced reductions in $|\vec{\nabla} P|$ are:

  small in core,

  largest at the pedestal top, $(0.93 < \Psi_N < 0.97)$,

  small (increase!?) at the edge.

- Key transport issue for ELM suppression is:

  How do RMPs reduce $|\vec{\nabla} P|$ at the pedestal top?

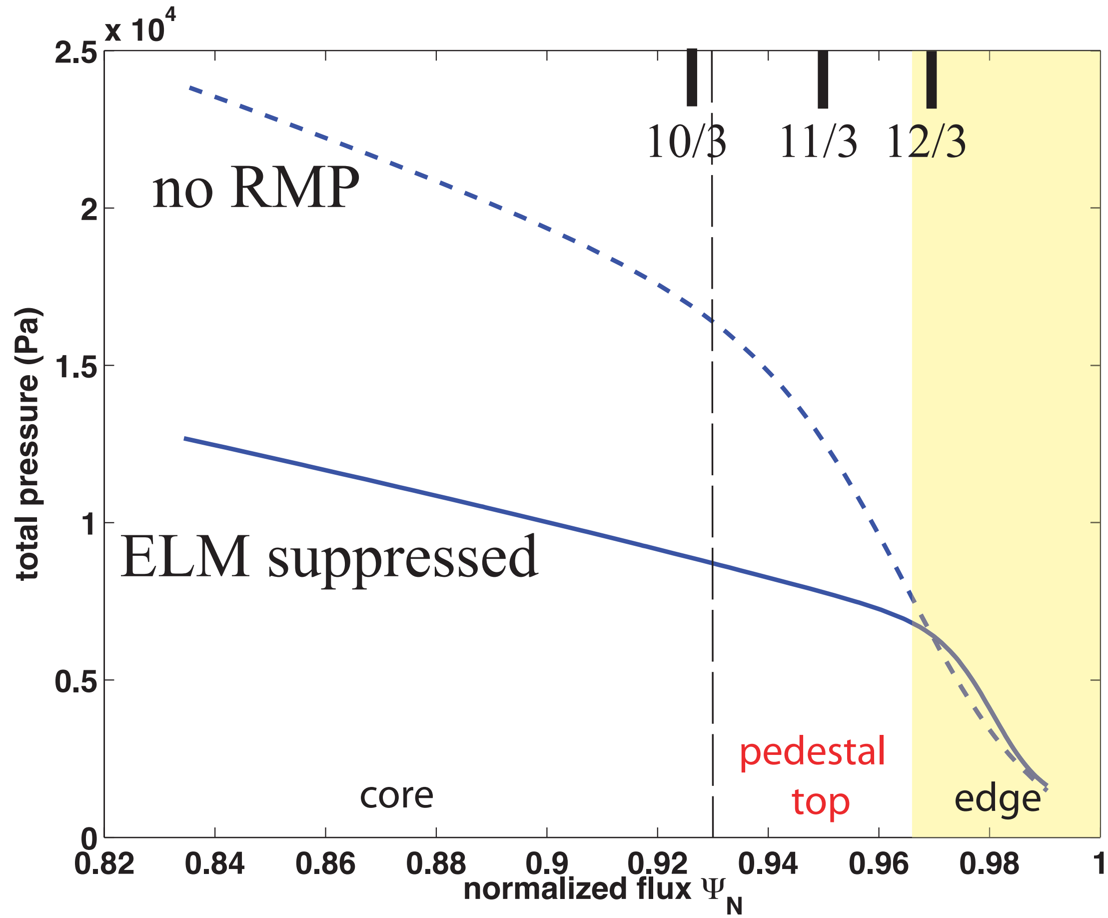

Figure 1: **Experimental pressure profile wo/with RMP ELM suppression. Courtesy of O. Schmitz, R. Nazikian, 2011. Indicated rational surface locations are approximate.**

How RMPs Suppress ELMs Is Not Yet Understood

- **Initial hypothesis[5] was that RMPs induce overlapping islands, magnetic stochasticity and Rechester-Rosenbluth[3] transport.**

- **But flow-screening[7] by extant toroidal flow in pedestals inhibits RMP "penetration," magnetic island formation & stochasticity — see Figs. 4 and 5 on p 16 and 17 at the end of this poster.**

- **Recent hypothesis[8] is RMPs induce an island slightly inward of the pedestal top which blocks inward expansion of the pedestal.**

- **RMP-induced magnetic flutter can induce additional radial electron transport[2,4] and reduce $\vec{\nabla} P$ throughout the pedestal top.**

- **This paper explores RMP-flutter-induced electron density and heat transport and its effects at the top of H-mode pedestals.**

---

[7]a) Y. Liu, A. Kirk, and E. Nardon, Phys. Plasmas **17**, 122502 (2010); b) M.S. Chu et al., Nucl. Fusion **51**, 073036 (2011); c) N.M. Ferraro, Phys. Plasmas **19**, 056105 (2012); d) M. Bécoulet et al., paper TH/2-1 at San Diego IAEA FEC, 8–13 October 2012; e) N.M. Ferraro et al., paper TH/P4-21.

[8]a) P.B. Snyder et al., Phys. Plasmas **19**, 056115 (2012); b) M.R. Wade et al., paper EX/3-1 at San Diego IAEA FEC, 8–13 October 2012.

RMPs Induce Radial Flutter Of Magnetic Field Lines

- **Between thin islands on rational surfaces, RMP fields cause sinusoidal radial (x,ρ) motion ("flutter") of magnetic field lines:**

  for $\vec{B} \equiv \vec{B}_0 + \delta\vec{B}$, $\hat{\vec{e}}_\rho \cdot \delta\vec{B} = \delta\hat{B}_{\rho\, m/n} \cos(m\theta - n\zeta)$, $\zeta = q(\rho)\,\theta = (m/n)\theta + xq'\theta$, integrating field line equation $dx/d\ell = (\delta\hat{B}_{\rho\, m/n}/B_0)\cos[k_\parallel(x)\,\ell]$, with $\ell \equiv R_0 q\,\theta$, $k_\parallel(x) \equiv -\,k_\theta\, x/L_S$, $k_\theta \equiv m/\rho$, $\boxed{x \simeq \rho - \rho_{m/n}}$ and $L_S \equiv R_0 q^2/(\rho q') = R_0 q/s$ (magnetic shear length) yields

$$\boxed{x(\ell) \simeq x_0 + \delta x(\ell), \text{ in which } \delta x(\ell) = \sum_{m,n} \frac{\delta\hat{B}_{\rho\, m/n}(x_0)}{B_0} \frac{\sin[k_\parallel(x_0)\ell]}{k_\parallel(x_0)}.}$$

- **Between rational surfaces the RMP-induced radial extent of sinusoidal radial variations of the "fluttering" field lines is**

$$2\max\{\delta x\} = \frac{\delta\hat{B}_{\rho\, m/n}(x_0)}{B_0} \frac{2}{k_\parallel(x_0)} \sim 5 \text{ mm}.$$

- **See Fig. 5 on p 17 at end of this poster for plot of radially fluttering field lines between isolated chains of magnetic islands.**

RMP-Flutter Induces Electron Thermal Diffusivity

- **Phenomenological plasma transport diffusivities D are**

  $$D \sim \frac{(\Delta x)^2}{2\,\Delta t}, \quad \text{for radial steps } \Delta x \text{ taken in a collision time } \Delta t \sim 1/\nu_e.$$

- **Electron collision damping at rate ν_e is critical for irreversibility.**

- **When electron collision length $\lambda_e \equiv v_{Te}/\nu_e$ is larger than $1/k_\parallel(x)$, which occurs outside thin layers around rational surfaces,**

  $$\text{for } k_\parallel(x)\lambda_e > 1, \quad \Delta x \sim \frac{1}{k_\parallel}\frac{\delta\hat{B}_{\rho\, m/n}}{B_0} \implies \boxed{D^{\text{RMP}} \sim \frac{\nu_e}{2\,k_\parallel(x)^2}\left[\frac{\delta\hat{B}_{\rho\, m/n}(x)}{B_0}\right]^2,}$$

  $$\text{which is applicable for } \boxed{|x| > \delta_\parallel \equiv \frac{L_S}{k_\theta \lambda_e} \sim 0.5 \text{ mm}} \text{ — off rational surfaces.}$$

- **$D^{\text{RMP}} \sim (1/x^2)\,\delta\hat{B}_{\rho\, m/n}(x)^2 \sim$ constant between rational surfaces since flow-screened $\delta\hat{B}^{\text{pl}}_{\rho\, m/n}(x) \sim |x|$ outside layer of width $\delta_\parallel$.**

RMP Plasma Transport Model Has Been Developed

- Collisional electron heat conduction along $\vec{B} = \vec{B}_0 + \delta\vec{B}$ produces Braginskii parallel electron heat flux $\vec{q}_{e\|} \equiv -(n_e \chi_{e\|}/B^2)\vec{B}\vec{B}\cdot\vec{\nabla}T_e$.

- Ideal MHD requires $\vec{B}\cdot\vec{\nabla}T_e = 0$ to lowest order for $|x| \gg \delta_\|$, which causes usual collisional $\vec{q}_{e\|}$ to vanish off rational surfaces.

- However, kinetic-based irreversible electron collisions plus RMP flutter[1,2,4] cause electron thermal diffusivity $\chi_e^{\delta B} \propto \chi_{e\|}^{\mathrm{eff}}\,(\delta B_\rho/B_0)^2$.

- Cylindrical[2] and toroidal[4] models of $\chi_{e\|}^{\mathrm{eff}}$ have been developed.

- The most relevant kinetic-based low collisionality toroidal model:[4]

  uses a Lorentz collision model,

  accounts for parallel flows only being carried by untrapped particles,

  resolves a collisional boundary layer in velocity space, and

  includes near-separatrix toroidal geometry and finite aspect ratio effects.

RMP-Flutter Induces Electron Transport Fluxes

- Toroidal model[4] RMP-flutter-induced radial transport fluxes of electron density $\Gamma_{et}^{\rm RMP} \equiv \langle \vec{\Gamma}_{et}^{\rm RMP} \cdot \vec{\nabla}\rho \rangle$ and heat $\Upsilon_{et}^{\rm RMP} \equiv \langle \vec{q}_{et} \cdot \vec{\nabla}\rho \rangle$ are

$$\boxed{\begin{bmatrix} \Gamma_{et}^{\rm RMP} \\ \Upsilon_{et}^{\rm RMP}/T_e \end{bmatrix} = -\,n_e \begin{bmatrix} D_{et}^{\rm RMP} & D_T^{\rm RMP} \\ \chi_n^{\rm RMP} & \chi_{et}^{\rm RMP} \end{bmatrix} \cdot \begin{bmatrix} d\ln \hat{p}_e/d\rho \\ d\ln T_e/d\rho \end{bmatrix}, \quad \frac{d\ln \hat{p}_e}{d\rho} = \frac{d\ln p_e}{d\rho} - \frac{e}{T_e}\frac{d\Phi_0}{d\rho},}$$

in which the total RMP-induced diffusivities are summed over all the m, n components:

$$\begin{bmatrix} D_{et}^{\rm RMP} & D_T^{\rm RMP} \\ \chi_n^{\rm RMP} & \chi_{et}^{\rm RMP} \end{bmatrix} = \sum_{mn} \begin{bmatrix} D_{et}^{m/n} & D_T^{m/n} \\ \chi_n^{m/n} & \chi_{et}^{m/n} \end{bmatrix} \equiv \frac{v_{Te}^2}{\nu_e}\frac{1}{2}\sum_{mn}\left(\frac{\langle \delta \hat{B}_{\rho\, m/n}^{\rm pl} \rangle}{B_{\rm t0}}\right)^2 \begin{bmatrix} K_{00} & K_{01} \\ K_{10} & K_{11} \end{bmatrix}.$$

The kinetically-derived Padé-approximate K_{ij} matrix of coefficients are defined by[4]

$$\begin{bmatrix} K_{00} & K_{01} \\ K_{10} & K_{11} \end{bmatrix} \equiv c_K \begin{bmatrix} G_{00} & G_{01} \\ G_{10} & G_{11} \end{bmatrix}, \quad \text{with coefficient } c_K \equiv \frac{B_{\rm t0}/B_{\rm max}}{\langle v_\parallel|_{\lambda=1}/v \rangle}\frac{13}{24\pi},$$

in which the matrix $G_{ij}(x)$ of dimensionless, spatially-dependent geometric coefficients are

$$\begin{bmatrix} G_{00} & G_{01} \\ G_{10} & G_{11} \end{bmatrix} \equiv \frac{4}{13\,|X|^{3/2}}\left(\frac{|X|^{3/2}}{c_{\parallel \rm t}}\int_0^{1/|X|^{1/2}} dy\, y^3 e^{-y} + \int_{y_{\rm min}}^{\infty} dy\, e^{-y}\right)\begin{bmatrix} 1 & y-\frac{5}{2} \\ y-\frac{5}{2} & (y-\frac{5}{2})^2 \end{bmatrix}, \quad c_{\parallel \rm t} = \frac{(3/16)(B_{\rm t0}^2/B_{\rm max}^2)}{f_c\, \langle v_\parallel|_{\lambda=1}/v \rangle},$$

$y_{\rm min} \equiv \max\{1/|X|^{1/2},\, 1/X_{\rm crit}^{1/2}\}$ and the normalized radial distance from m/n rational surface is

$$\boxed{X \equiv \frac{x}{\delta_{\parallel \rm t}} = \frac{q(\rho) - m/n}{q'\, \delta_{\parallel \rm t}} \simeq \frac{\rho - \rho_{m/n}}{\delta_{\parallel \rm t}}} \quad \text{in which } \delta_{\parallel \rm t} \equiv c_{\rm t}\frac{L_S}{k_\theta\, \lambda_e}, \quad \text{with } c_{\rm t} \equiv 3\sqrt{\pi}\,|\langle v_\parallel|_{\lambda=1}/v \rangle|\frac{B_{\rm max}}{B_{\rm t0}}.$$

RMP Fluxes Have Diverse Parameters And Properties

- **In low collisionality DIII-D plasmas in which RMPs suppress ELMs,[2,5] typical pedestal top parameters at $\Psi_N \simeq 0.95$ are[4]**

  $T_e \simeq 1130$ eV, $n_e \simeq 2.5\times 10^{19}$ m^{-3}, $Z_{\rm eff} \simeq 1.7$, $\lambda_e \simeq 350$ m, $v_{Te}^2/\nu_e \simeq 7\times 10^9$ m$^2\cdot$ s^{-1}, $\langle \delta \hat{B}^{\rm vac}_{\rho\, m/n}\rangle / B_{\rm t0} \simeq 3.34\times 10^{-4}$, $B_{\rm max}/B_{\rm t0} \simeq 4/3$, $\langle v_\parallel|_{\lambda=1}/v\rangle \simeq 0.45$, $c_K \simeq 0.29$, $X_{\rm crit} \equiv (2/3\sqrt{\pi})\,(B_{\rm t0}/B_{\rm max})(\lambda_e/R_0 q) \simeq 17$, $c_{\parallel \rm t} \simeq 0.94$, $c_t \simeq 3.2$, $L_S \simeq 2.4$ m, $k_\theta \simeq 15$ m^{-1}, $\rho_{11/3} - \rho_{10/3} \simeq 1/nq' \simeq 2.8$ cm and $\boxed{\delta_{\parallel \rm t} \simeq 1.5 \text{ mm.}}$

- **RMP-flutter-induced radial transport fluxes:**

  are Onsager-symmetric for thermodynamic forces $d\ln \hat{p}_e/d\rho$ and $d \ln T_e/d\rho$,

  include contributions both inside dissipative layer and outside ($|x| \gg \delta_{\parallel \rm t}$) it,

  have parallel diffusivities that decrease as $|x|^{-3/2}$ due to collisional boundary layer and are large near rational surfaces but smaller between them,

  have larger thermal than density diffusivites ($\chi_{\rm et}^{m/n}/D_{\rm et}^{m/n} \simeq 3.25$),

  have negative off-diagonal components ($D_T^{m/n}/D_{\rm et}^{m/n} \simeq \chi_n^{m/n}/\chi_{\rm et}^{m/n} \simeq -3/2$) off of rational surfaces ($|x| \gg \delta_{\parallel \rm t}$) due to thermal and frictional forces.

More Effects Are Included In Comparisons To Data

- **Requiring electron particle flux to be ambipolar yields a reduced effective electron thermal diffusivity $\chi_{e\,\mathrm{eff}}^{m/n}$ for $|x| \gg \delta_{\parallel \mathrm{t}}$:**

$$\Gamma_{\mathrm{et}}^{m/n} = -\,n_e \left(D_{\mathrm{et}}^{m/n} \frac{d\ln \hat{p}_e}{d\rho} + D_T^{m/n} \frac{d \ln T_e}{d\rho} \right) \to 0 \quad \Longrightarrow \quad \frac{d\ln \hat{p}_e}{d\rho} = -\,\frac{D_T^{m/n}}{D_{\mathrm{et}}^{m/n}} \frac{d\ln T_e}{d\rho},$$

which yields effective electron thermal diffusivity off rational surfaces:

$$\chi_{e\,\mathrm{eff}}^{m/n} = \chi_{\mathrm{et}}^{m/n} \left[1 + \left(\frac{\chi_n^{m/n}}{\chi_{\mathrm{et}}^{m/n}} \right) \left(-\frac{D_T^{m/n}}{D_{\mathrm{et}}^{m/n}} \right) \right] \simeq \frac{4}{13}\, \chi_{\mathrm{et}}^{m/n} \text{ — factor of 4/13 smaller.}$$

- **Magnetic island of width W modifies $\chi_e^{m/n}(\rho)$ near rational surface:**

preceding analysis is only valid outside island, $x_0 \gg W/4 \equiv [\delta \hat{B}_{\rho\, m/n} L_S / k_\theta B_0]^{1/2}$,

effective radial electron thermal diffusivity near island will be estimated by

$$\chi_{eW\mathrm{eff}}^{m/n} \simeq \frac{1}{\frac{1-F_W^{m/n}(x)}{\chi_{e\,W}^{m/n}} + \frac{F_W^{m/n}(x)}{\chi_{e\,\mathrm{eff}}^{m/n}(x)}}, \qquad F_W^{m/n}(x) = \begin{cases} 0, & |x| < W/4 \\ \frac{|x| - W/4}{W/4}, & W/4 \le |x| \le W/2 \\ 1, & |x| > W/2 \end{cases},$$

in which $\chi_{e\,W}^{m/n} \sim \infty$ is thermal diffusivity across island region.

T_e Profile Between m/n Surfaces Is Caused By $\chi_{eW\,\mathrm{eff}}^{m/n}(\rho)$

- Model flow-screened RMPs with

$$\delta\hat{B}^{\mathrm{pl}}_{\rho\, m/n}(x) = \delta\hat{B}^{\mathrm{vac}}_{\rho\, m/n}\left(\frac{1}{f_{\mathrm{scr}}^2} + \frac{x^2}{L_{\delta B}^2}\right)^{1/2},\ L_{\delta B} \simeq 2.5\,\mathrm{cm},$$

with flow-screening factor $f_{\mathrm{scr}} \equiv \dfrac{\delta\hat{B}^{\mathrm{vac}}_{\rho\, m/n}(0)}{\delta\hat{B}^{\mathrm{pl}}_{\rho\, m/n}(0)}$.

- Parameters for Figs. 2 and 3 are[4]

$f_{\mathrm{scr}} = 4$ and $W \simeq 1.5$ cm.

- $\chi_{e\,\mathrm{eff}}^{\mathrm{RMP}}$ (dashed) and $\chi_{e\,W\mathrm{eff}}^{\mathrm{RMP}}$ (solid) obtained by adding 10/3 and 11/3 contributions are shown in Fig. 2.

- Resultant T_e profile is in Fig. 3.

- Dotted lines in Figs. 2 and 3 show radially-averaged $\overline{\chi}_e^{\mathrm{RMP}}$ from $\Delta T_e/\Delta\rho$.

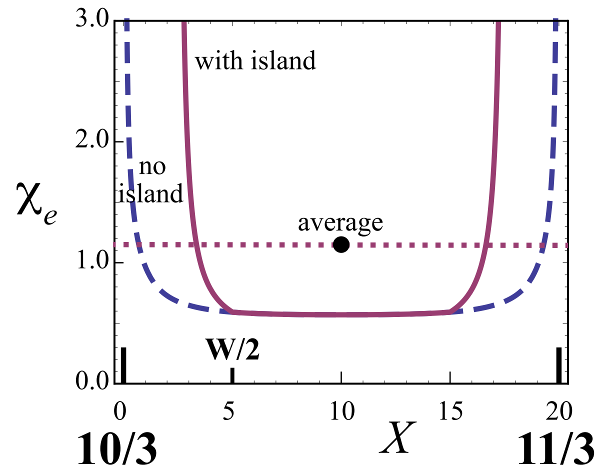

Figure 2: Radial variation of χ_e^{RMP}.

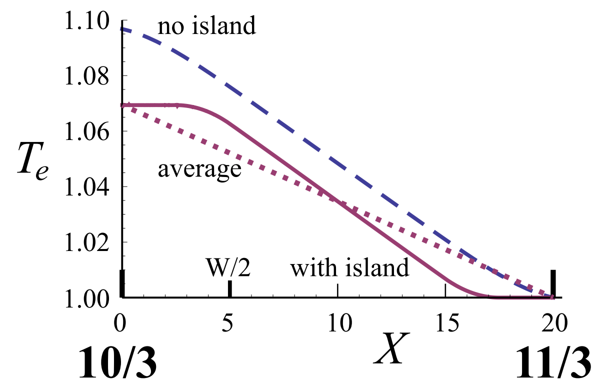

Figure 3: Predicted T_e profile.

Radially-Averaged $\overline{\chi}_e^{\rm RMP}$ Is Comparable To DIII-D Data

- **While large $\chi_e^{\rm RMP}$ at rational surfaces flattens the T_e profile there, average $dT_e/d\rho$ is determined mainly by the minimum diffusivity — radial heat flow is like resistors with impedance $1/\chi_e$ in series.**

- **Radially-averaged $\overline{\chi}_e^{\rm RMP} \simeq 1.15$ m$^2\cdot$ s^{-1} with islands is larger than $\chi_{e\,\rm exp}^{\rm sym} \simeq 0.6$ m$^2\cdot$ s^{-1}, which should reduce $dT_e/d\rho$ at pedestal top.**

- **However, it is smaller than the experimental[2] $\chi_{e\,\rm exp}^{\rm RMP} \sim 4$ m$^2\cdot$ s^{-1}.**

- **Predicted $\overline{\chi}_e^{\rm RMP}$ would be larger if**

  other m/n contributions are included (usually small effect), or

  flow-screened RMP fields $\delta\hat{B}^{\rm pl}_{\rho\, m/n}$ obtained from extended MHD codes such as M3D-C1[7c,e] are used in the diffusivity evaluations, which are underway[9] — see last 3 viewgraphs at the end of this poster.

[9] P.T. Raum, S.P. Smith, J.D. Callen, N.M. Ferraro, O. Meneghini et al., "Comparison of flutter model with DIII-D RMP data" (to be presented in poster JP8 17 at the Providence APS-DPP meeting, Oct. 29 – Nov. 2, 2012 and to be published).

Radial Electric Field Is Determined By Torque Balance

- Since RMP-induced ion density flux $\sim \nu_i$ is smaller by a factor of $(m_e/m_i)^{1/2} \sim 1/60$, RMPs induce a radial current $J_\rho^{\mathrm{RMP}} < 0$.

- Non-ambipolar (na) radial density fluxes cause[10] toroidal torque densities ($T_\zeta \equiv \vec{e}_\zeta \cdot \vec{F}_{\mathrm{orce}}$ where $\vec{e}_\zeta \equiv R^2 \vec{\nabla}\zeta = R\,\hat{\vec{e}}_\zeta$) on the plasma:

  $T_\zeta = -\,q_s\,\langle \vec{\Gamma}_s^{\mathrm{na}} \cdot \vec{\nabla}\psi_{\mathrm{p}} \rangle = -\,q_s\,\langle \vec{\Gamma}_s^{\mathrm{na}} \cdot \vec{\nabla}\rho \rangle\,\psi_{\mathrm{p}}'$ — function of $E_\rho \equiv -|\vec{\nabla}\rho|\,d\Phi_0/d\rho$.

- Ion & electron 3D density fluxes cause oppositely directed torques:

  $\vec{\Gamma}_i^{\mathrm{na}}$ (NTV, ripple) create[10d] counter-current torques because $q_i = +\,e$ ($J_\rho > 0$), but RMP electron density fluxes create co-current torques because $q_e = -\,e$.

- Torque density equation for $L_{\mathrm{t}} \equiv m_i n_i \langle R^2 \rangle \Omega_{\mathrm{t}}$ sums all torques:[10]

$$\underbrace{\frac{\partial L_t}{\partial t}}_{\text{inertia}} \simeq -\underbrace{\langle \vec{e}_\zeta \cdot \vec{\nabla} \cdot \overleftrightarrow{\pi}_{i\parallel}^{\,3\mathrm{D}} \rangle}_{\text{NTV from } \delta B_\parallel} + \underbrace{\langle \vec{e}_\zeta \cdot \overline{\delta \vec{J} \times \delta \vec{B}} \rangle}_{\text{resonant } \delta \vec{B}\text{s}} - \underbrace{\langle \vec{e}_\zeta \cdot \vec{\nabla} \cdot \overleftrightarrow{\pi}_{i\perp} \rangle}_{\text{cl, neo, paleo}} - \underbrace{\frac{1}{V'}\frac{\partial}{\partial \rho}\left(V' \Pi_{i\rho\zeta}\right)}_{\text{Reynolds stress}} + \underbrace{\langle \vec{e}_\zeta \cdot \textstyle\sum_s \overline{\vec{S}}_{sm} \rangle}_{\text{mom. sources}} .$$

[10] a) J.D. Callen, A.J. Cole and C.C. Hegna, Nucl. Fusion **49**, 085021 (2009); b) J.D. Callen, A.J. Cole and C.C. Hegna, Phys. Plasmas **16**, 082504 (2009); c) J.D. Callen, C.C. Hegna and A.J. Cole, Phys. Plasmas **17**, 056113 (2010); d) J.D. Callen, Nucl. Fusion **51**, 094026 (2011).

Ambipolar Constraint Predicts Radial Electric Field

- **RMP-flutter-induced toroidal torque density is**

$$\langle \vec{e}_\zeta \cdot \overline{\delta \vec{J}_\parallel \times \delta \vec{B}_\rho} \rangle = e\,\Gamma_e^{\rm RMP} \psi_{\rm p}' = -\frac{n_e m_i}{\rho_S^2/R^2} \sum_{mn} D_{\rm et}^{m/n} (\Omega_{\rm t} - \Omega_{*e}), \qquad \frac{\rho_S^2}{R^2} = \frac{T_e/m_i}{e^2 \psi_{\rm p}'^2/m_i^2},$$

$$\Omega_{e*} \equiv -\frac{1}{e}\left(\frac{1}{n_e}\frac{dp_e}{d\psi_{\rm p}} + \frac{1}{n_i}\frac{dp_i}{d\psi_{\rm p}} + \frac{D_T^{m/n}}{D_{\rm et}^{m/n}}\frac{dT_e}{d\psi_{\rm p}}\right) + \Omega_{\rm p} \sim -\frac{1}{n_e e R B_{\rm p}}\frac{dP}{d\rho} > 0.$$

- **If this torque is dominant, RMP-induced electron flux vanishes $\Longrightarrow$ ambipolarity constraint, $\Omega_{\rm t} \simeq \Omega_{e*}$ and radial electric field:**

$$\vec{E}_0 \equiv -\vec{\nabla}\rho \frac{d\Phi_0}{d\rho} \simeq -\vec{\nabla}\rho \frac{T_e}{e}\left(\frac{d\ln p_e}{d\rho} - \frac{3}{2}\frac{d\ln T_e}{d\rho}\right).$$

- **These "electron root" predictions are consistent with DIII-D data:**[11]

  radial electric field changes from $-$ to $+$ for $\Psi_N \lesssim 0.93$, and

  $\Omega_{\rm t}$ "jumps" to $\Omega_{e*} \sim 10\ \mathrm{kRad \cdot s^{-1}}$ at $\Psi_N \sim 0.95$ when[4,11] RMPs suppress ELMs.

[11] R.A. Moyer et al., "Comparison of Plasma Response Models to Measurements in DIII-D RMP H-mode Discharges," poster TP9 3 at Salt Lake City APS-DPP Meeting, Nov. 14-18, 2011.

RMP Effects Are Different At High Collisionality

- **ASDEX-U[6] electron collision frequency ν_e is $\gtrsim\times 10$ greater which**

  1) increases shear-effects width parameter by a factor $\sim \times 10$ to $\delta_\parallel \gtrsim 2$ cm,

  2) causes most "smoothing" processes to exceed half the distance between rational surfaces and hence overlaps the effects around various m/n surfaces $\Longrightarrow q_{95}$ resonance effects and magnetic islands are less likely.

  3) reduces bootstrap current and possibly $\delta \hat{B}^{\rm pl}_{\rho\, m/n}$ RMP responses.

  4) makes transition to "electron root" unlikely because m/n effects overlap and increased edge NBI momentum input makes usual ion root more robust.

- **Model predictions for approximate ASDEX-U conditions[6] are:**

  1) $\chi_e^{\rm RMP} \sim \nu_e L_S^2 \sum_{mn} \left[\dfrac{\delta \hat{B}^{\rm vac}_{\rho\, m/n}}{B_0}\right]^2 \gtrsim 1~{\rm m^2/s}, \quad L_S \equiv \dfrac{R_0 q}{s}$ **magnetic shear length,**

  2) which reduces gradients throughout pedestal if it exceeds a typical level of $D_\eta \sim \eta/\mu_0 \sim \nu_e \delta_e^2$ transport there and yields an ELM mitigation criterion:

$$\delta_e^2 \equiv \frac{c^2}{\omega_{pe}^2} \simeq \frac{3\times 10^{19}}{n_e({\rm m^{-3}})} 10^{-6} \;\lesssim\; L_S^2 \sum_{mn} \left[\frac{\delta \hat{B}^{\rm vac}_{\rho\, m/n}}{B_0}\right]^2 \quad \Longrightarrow \quad n_e \gtrsim 5\times 10^{19}~{\rm m^{-3}}?$$

SUMMARY: RMP-Flutter Transport Is New Paradigm

- **New model for RMP-flutter-induced electron density and heat fluxes (p 7) has been developed and is beginning to be tested.[2,4,9]**

- **Requiring density flux to be ambipolar yields predictions for effective thermal diffusivity (p 9) and pedestal electric field (p 13).**

- **Effects of thin islands at rational surfaces are estimated (p 9).**

- **Fig. 2 shows while χ_e^{RMP} in low collisionality pedestals is largest at rational surfaces, Fig. 3 shows ΔT_e between them and $\overline{\chi}_e^{\mathrm{RMP}}$ depend mainly on minimum diffusivity midway between surfaces.**

- **Model predictions agree semi-quantitatively with DIII-D results — for $\overline{\chi}_e^{\mathrm{RMP}}$, average $dT_e/d\rho$ and E_ρ at pedestal top.**

- **RMP-flutter-induced transport could reduce pedestal top $|\vec{\nabla} P|$, limit its expansion and stabilize P-B instabilities, suppress ELMs.**

M3D-C1 Provides RMP-Fields In Plasma, TH/P4-21 $\Longrightarrow$

- **RMP-induced m/n fields:**

  are reduced from vacuum values on rational surfaces,

  by flow-screening factor $f_{\rm scr}$, but

  grow $\sim$ linearly away from them.

- **Parameters of the highlighted 11/3 RMP field are**

  $f_{\rm scr} \sim 10$,

  $L_{\delta B} \sim 0.02\,a$
  ~ 1.6 cm.

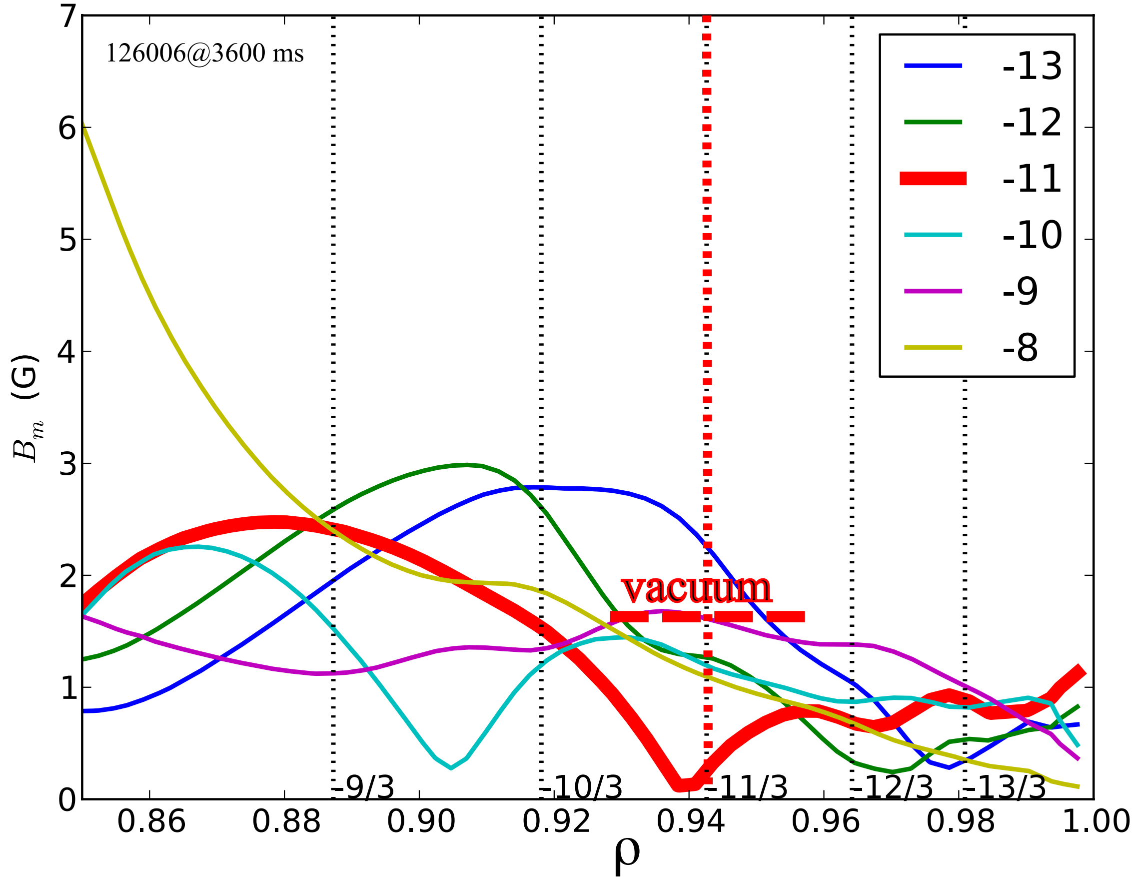

Figure 4: **Flow-screened RMP-induced $\langle \hat{B}^{\rm pl}_{\rho\, m/n} \rangle$. Courtesy of N.M. Ferraro, O. Meneghini and S.P. Smith 2012.**

Plasma Response To RMPs Creates Radially Isolated Island Chains With Magnetic Flutter Between Them

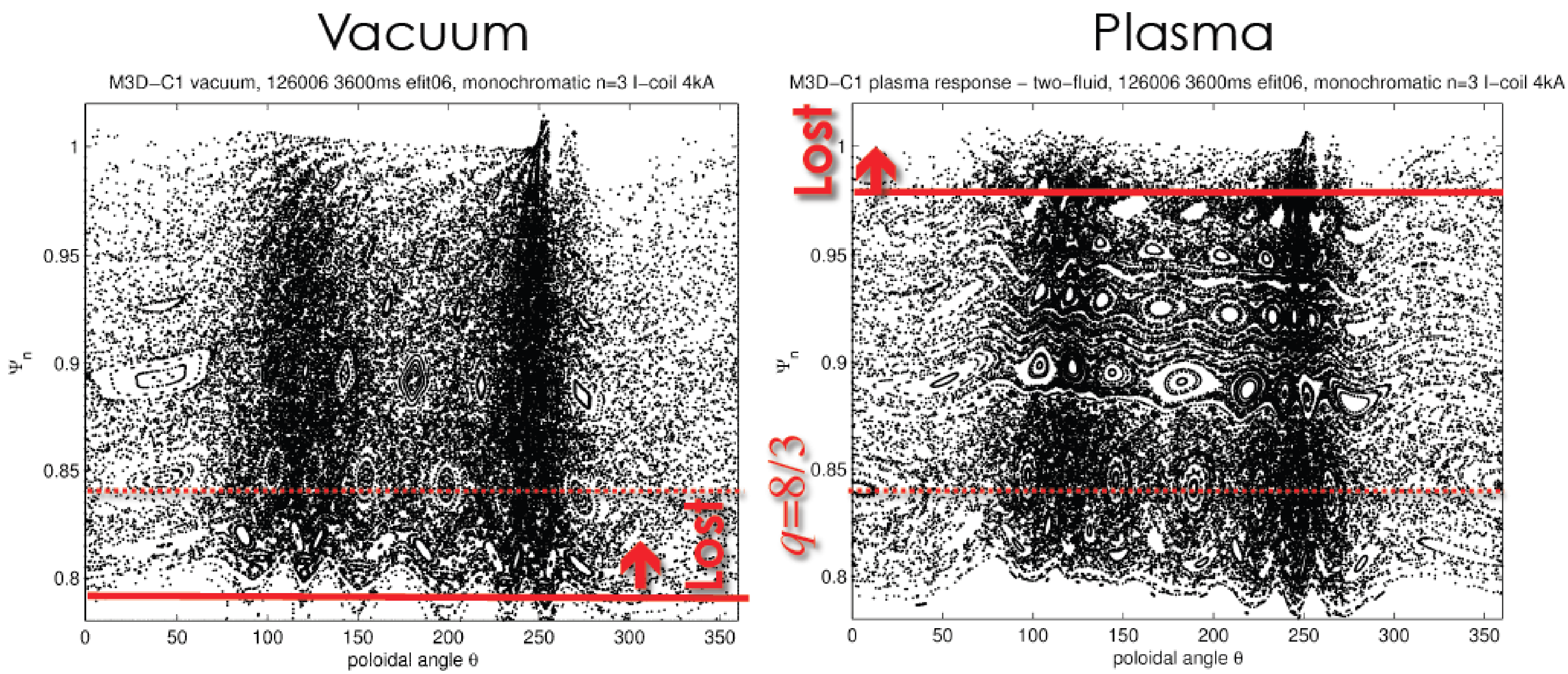

Figure 5: **Poincare plots of field lines with vacuum RMP fields (left) and with flow-screened RMP plasma response fields (right) from M3D-C1 $\langle \delta \hat{B}^{\rm pl}_{\rho\, m/n} \rangle$ shown in Fig. 4. Figures courtesy of D. Orlov, R.A. Moyer and N.M. Ferraro, 2012.**

Flutter Model χ_e and T_e Profiles Using Preceding RMP Fields Are Consistent With Experimental Profiles

- **Figures courtesy of S.P. Smith, P.T. Raum (NUF student), N.M. Ferraro and O. Meneghini (see reference 9 on p 11).**

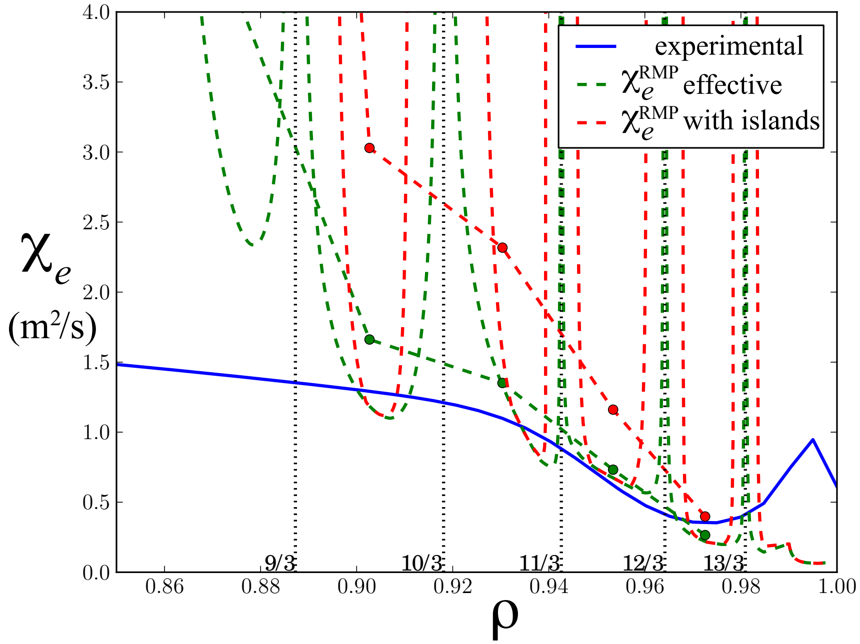

Figure 6: **Electron thermal diffusivity profiles for the two flutter models in the edge of DIII-D discharge 126006.**

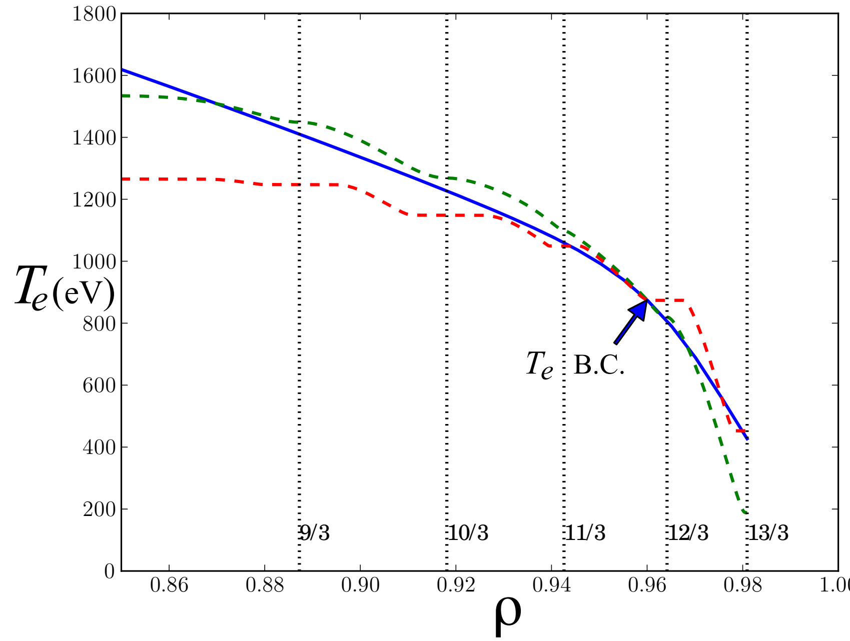

Figure 7: **Corresponding T_e profiles for the two flutter models in the edge of DIII-D discharge 126006.**